



## Vacuum membrane distillation for deep seawater: experiments and theory

Ho Ji<sup>a</sup>, Mi-Yeon Choi<sup>a</sup>, Ho-Seng Lee<sup>a</sup>, Albert S. Kim<sup>b</sup>, Hyeon-Ju Kim<sup>a,\*</sup>

<sup>a</sup>Seawater Utilization Plant Research Center (SUPRC), Korea Research Institute of Ships and Ocean Engineering, Goseong-gun, Gangwon-do 219-822, Korea, Tel. +82-33-630-5000; Fax: +82 33 630 5005; email: hyeonju@kriso.re.kr

<sup>b</sup>Civil and Environmental Engineering, University of Hawaii at Manoa, 2540 Dole Street Holmes 383, Honolulu, Hawaii 96822, USA

Received 23 December 2015; Accepted 9 May 2016

---

### ABSTRACT

This paper investigates the feasibility and potential of vacuum membrane distillation (VMD) for concentrating deep seawater (DSW) of 34 g/kg and its reverse osmosis (RO) brine of 62 g/kg. In this work, a small pilot-scale VMD system was developed and distillate fluxes were measured for feed solutions of de-ionized water (DIW), DSW and RO brine. DIW provided the highest distillate flux followed by DSW and RO brine, but effects of feed salinity on the flux is not remarkable. A simple analysis was performed using conventional mass transfer theory, which provides good qualitative understanding of relative fluxes of DSWs normalized by that of DIW. The experimental observation indicated that VMD can be readily used for desalination and concentration of salinity solutions as high as 62 g/kg. This supports great potential of VMD for membrane crystallization of precious DSW minerals.

*Keywords:* Vacuum membrane distillation; Membrane crystallization; Deep seawater; Reverse osmosis brine; Ocean thermal energy conversion

---

### 1. Introduction

Membrane distillation (MD) is one of the emerging isothermal separation technologies for seawater and brackish water desalination [1]. MD has great potential to reduce net energy consumption as a replacement or supplement to energy-intensive processes such as reverse osmosis (RO) and thermal distillation [2]. The cost-effectiveness of MD depends on availability of inexpensive heat sources to maintain hot feed temperature [3]. The driving force for MD is the partial pressure gradient of water vapor along membrane pores. The partial pressure at the feed-membrane interface is approximated as the water saturation pressure in equilibrium with the hot feed temperature. At the membrane-distillate interface, the partial pressure is determined by condensing schemes, which categorize MD types of direct contact membrane distillation (DCMD), vacuum membrane distillation (VMD), sweep gas membrane distillation (SGMD), and air-gap membrane distillation (AGMD) [2,4].

VMD maintains a low pressure or (near) vacuum on the distillate (permeate) side by means of vacuum pumps. In the vacuum phase, the gas phase pressure is a few percent of the atmospheric pressure, which is often defined as a low-quality vacuum in vacuum science and technology. This vacuum pressure should be maintained (much) lower than the water saturation pressure at the feed-membrane interface. An external condenser is required for phase change of water from vapor to liquid, which is usually installed between the membrane module and the vacuum pump. DCMD is more widely studied and used due to easy setup, installation, and operation without external condensers. In addition, SGMD uses dry or ambient air flow to sweep and condense the water vapor using external condensers. Advantages of VMD over DCMD include lower conductive heat loss and lower mass transfer resistance. The vacuum phase is an excellent thermal insulator, and therefore the thermal boundary layer barely forms at the membrane-vacuum interface. Note that thermal conductivities of the feed solution, a membrane

---

\* Corresponding author.

consisting of solid and humid air, and vacuum phases are of orders of  $O(10^3)$ ,  $O(10^2)$ ,  $O(10^1)$  mW/m<sup>2</sup> K, respectively. Detailed multi-scaling analysis of MD can be found elsewhere [5]. Another big difference between VMD and DCMD is the gaseous composition in the pore spaces. Humid air (a mixture of dry air and evaporated water) is stagnant in pore spaces in DCMD processes. The gas phase is (literally) confined by solid pore-walls and two interfacial liquid streams. The rejection of solute components, especially salt ions for desalination, is as good as that of RO, (almost) regardless of chemical and physical characteristics of the salt ions [6]. This is because the extraction mechanism of MD is the selective evaporation of water over solutes at a low temperature (below the boiling point of 100°C at 1 atm), which is followed by condensation of the water vapor at liquid or solid surfaces. The vapor pressure of the saline water is indifferent to charge valence and molecular weight of solutes, and the pH of the feed solution. Vapor pressure of seawater is a weakly decreasing function of the salt concentration [7].

Being superior to other MD processes, VMD has a higher probability to face pore wetting due to the stronger driving force of the applied vacuum [8]. Polydispersity of the pore size distribution is the key factor in causing membrane wetting, of which in-depth qualitative analysis can be found elsewhere [8]. Unlike DCMD, the wetting of VMD does not directly influence solute rejection. Water penetrating through VMD membranes (by wetting) will not transport to the external condenser, but remains inside the module instead. Some fraction of this penetrated water may evaporate while being retained inside the module. Operations can be temporarily ceased to drain the retained water and membranes can be dried for cleaning purpose. Although VMD is less prone to membrane wetting, it consumes much more (electric) energy to maintain the low gas pressure on the distillate side. The energy consumption rate is highly correlated to the non-linear variation of the saturation pressure with respect to the liquid-phase (feed) temperature. For example, Criscuoli et al. [9] reported that increasing the vacuum pressure from 10 to 60 mbar decreases the energy consumption 1.97 times. Taking the vacuum pressures as saturation pressures, one calculates the corresponding equilibrium temperatures of 6.25°C and 36.4°C (for the vacuum pressures of 10 and 60 mbar, respectively), which can be considered as theoretical minimum values of feed temperatures. It is often required to reduce the vacuum pressure below 30–40 mbar, which requires higher energy consumption of VMD in comparison with other MD types. Future applications of VMD include ocean thermal energy conversion (OTEC) for simultaneous or alternative generation of electricity and fresh water [10]. OTEC uses the temperature gradient between the surface (20°C–30°C) and deep (4°C–8°C) ocean water for evaporation and condensation, respectively. A significant drawback of the OTEC technology is the extraordinarily large scales of instruments and equipment. Our previous estimation indicates that use of VMD modular systems as a replacement of the conventional evaporator can significantly reduce the total evaporator volume to as low as 10% [11]. Although RO is currently the most popular desalination technology, providing the world least expensive cost below \$50/ton of desalinated water [12], an unavoidable problem is brine disposal, which initiates environmental concerns

and makes environmental regulations more stringent. Current technologies for seawater concentration and mineral extraction rely on RO and low-pressure evaporation, but a disadvantage is the considerable energy consumption and (unreasonably) high concentration and temperature of disposed brine. As the brine solution has (much) higher salt concentration than the seawater, additional use of RO stages are very energy-intensive for concentrating brine solutions near the solubility limit. Other options include conventional evaporation and crystallization, which are still not cost-effective due to the high energy consumption and vulnerability to corrosion [13,14]. Inorganic precipitation during membrane separation initiates deleterious fouling followed by noticeable flux decline. If the precipitation occurs, however, away from the membrane surface and precipitated salts are separately collected, MD can be used for solution concentration as well as mineral extraction. In this light, membrane crystallization (MCR) may offer an attractive alternative solution to a combination of membrane distillation (MD) and a separate crystallizer. MCR was first studied for concentrated salt solutions by Wu and Drioli [15], who observed precipitation of crystal solutes outside the membrane module. Curcio et al. [16] addressed the application of MCR for crystallization of sodium chloride. Transmembrane flux was low on purpose by maintaining feed and distillate inlet temperatures of 29°C and 9°C, respectively. This is to minimize the concentration polarization and so prevent precipitation-induced fouling on the membrane surface. In MCR processes, fresh water is produced as permeate from the MD process, while the concentrated solutes can be recovered as solids from the crystallizer [17–19]. At present, the challenging part of MCR is controlling the hot feed temperature to increase downstream concentration for crystallization without causing precipitation on the membrane surface.

Seawater Utilization Plant Research Center (SUPRC), located at Goseung-gun, Gangwon-do, the north-most part along the East Sea side of Korea, has been devoted to DSW R&D for practical technologies and commercial applications. DSW is continuously pumped from 500 m below the ocean surface using 5 km of high-pressure pipes. Physical, chemical, and health-related characteristics of this deep seawater (DSW) can be found elsewhere [20–22]. Currently, the DSW is desalinated using high-pressure RO systems and commercialized as drinking water by Gangwon Deep Sea Water Co., Ltd, located beside SUPRC. In general, salt concentration does not noticeably change with respect to the depth of ocean. DSW contains the same salt concentration and composition as those of the surface seawater, but lower contents of microbial entities, suspended solids, and particulate matter. This implies that fouling potential must be less than the surface seawater for conventional desalination using RO or thermal processes. Eykens et al. [23] successfully applied DCMD for desalination of synthetic seawater of various concentrations (i.e., NaCl of 0, 13, and 23 wt%) and reported the presence of optimal thickness of flat sheet MD membranes. Their experimental results strongly imply the great possibility of using MD for secondary concentration of highly saline solutions. A unique feature of the current research is to investigate the potential of VMD for energy efficient desalination and high-degree concentration of DSW, which will significantly reduce brine volume. Experimental observation of the

current research will be extended in the future to MCr for high-purity mineral extraction.

Our specific interest is to concentrate the brine solution near the solubility limit to reduce the brine volume, followed by recovering precious salt and mineral ions using energy-efficient technologies. In this study, the VMD performance using DSW and its RO brines as feed solutions was investigated for desalination performance of VMD and its future potential to crystallize minerals from DSW.

## 2. Materials and methods

### 2.1. Materials

#### 2.1.1. Membrane

Typical materials used to prepare MD membranes include polytetrafluoroethylene (PTFE), PVDF, and polypropylene (PP), and their thermal conductivities range from 0.11 to 0.29 from temperature 296 to 348 K [24]. Polyvinylidene fluoride (PVDF) membranes of the hollow fiber type were supplied by Ecomity Inc. Korea. Detailed technical information of the membrane can be found in Table 1. The membranes have average inner and outer radius of 0.35 and 0.60 mm, respectively, and the thickness is calculated as 0.25 mm. The vendor provided physical and chemical characteristics of the membrane, which are pore diameter, porosity, thermal conductivity, and contact angle, and liquid entry pressure (LEP). PVDF LEP varies typically from 105 to 204 kPa (i.e., 1.05 and 2.04 bar, respectively) [2]. The prepared membrane in this study has a LEP of 1.60 bar, which is in our opinion a reasonable for VMD operations.

#### 2.1.2. Module

Fig. 1 shows a membrane module consisting of a cylindrical vessel and a number of hollow fibers. In Fig. 1(a), 180 hollow fibers of 17 cm in length are packed in parallel to the inner vessel-wall, and each side was ported rigidly to the vessel. The module is temporarily detached from the system.

Table 1

Characteristics of hollow fiber membranes

	Variables	Values	Unit
	Pore diameter, $d_p$	0.10	$\mu\text{m}$
	Membrane porosity, $E$	0.70	[-]
	Thermal conductivity, $\kappa$	0.2	W/m K
	Liquid entry pressure (LEP)	1.60	bar
	Contact angle, $\theta_c$	$105 \pm 5$	$^\circ$
Membrane	Inner diameter, $D_i$	0.70	mm
	Outer diameter, $D_o$	1.20	mm
	Thickness, $\delta_m$	0.25	mm
	Number of fibers, $N_{hf}$	180	ea.
	Fiber length (ea.), $l_f$	0.17	m
	Total fiber length, $L_f$	30.6	m
	Total surface area	$A_{mi} = 0.0673$	$\text{m}^2$
		$A_{mo} = 0.1154$	$\text{m}^2$

The hollow fibers were ported at each end of the containing vessel. Two small holes of 10 mm in diameter were made at opposite ends of the vessel surface to extract water vapor from the interior to the condenser: one on the top-left side and the other on the bottom-right side of the vessel. Only one hole is shown at the upper part of Fig. 1(a) because the second hole is behind the vessel. Fig. 1(b) shows the module installed in the VMD system. Arrows in Fig. 1(b) are physically marked on tubes of the VMD system (not digitally illustrated on the image), and one arrow on a tube connected to the top-left hole is not shown since it is behind the tube. The hot feed stream was introduced from the bottom side of the vessel and flowed upward through membrane lumen spaces. The direction of feed flow is indicated by two vertical arrow stickers attached on tube surfaces below and above the vessel. The effective length of each membrane, excluding the ported parts, is 17 cm. The total membrane length within the vessel is calculated as 30.6 m. Membrane surface areas are calculated using the inner and outer diameters,  $D_i$  and  $D_o$ , denoted as  $A_{mi}$  and  $A_{mo}$ , respectively. The outer membrane surface area  $A_{mo}$  is approximately twice the inner membrane surface area  $A_{mi}$ . Since the hot feed is introduced to the lumen space,  $D_i$  was used to calculate the total surface area. Fundamental discussion about flux calculation of hollow fiber membrane can be found elsewhere [24].

#### 2.1.3. Feed solutions

Three types of feed solutions were tested: de-ionized water (DIW) and DSW of 34 and 62 g/kg, denoted as DSW34 and DSW62, respectively. DIW was prepared using a pure water generator (model: MR-RO1600) from MiRAEST Co., Ltd, Korea, consisting of a pretreatment unit (model: PCPF005S), an activated carbon filtration unit (model: PCAC010S), and a small RO system (model: PCRM1075). DSW was obtained by pumping seawater from 500 m below the ocean surface at SUPRC, located at Goseong-gun, Gangwon-do, Korea. The concentration of this raw DSW was measured as 34.0 g/kg, and detailed information can be found elsewhere [20,22].



Fig. 1. Photo images of (a) a detached module of 180 PVDF hollow fibers and (b) the same module connected to a feed tank and a vacuum pump in the VMD system.

The concentrated DSW62 is provided by Gangwon Deep Sea Water Co., Ltd., located beside SUPRC. Their DSW was pumped at the same location, but at 600 m in depth. An RO system was used to desalinate the DSW34 and DSW62 is the RO brine to be disposed in the ocean.

2.2. Methods

Fig. 2 shows a schematic of the VMD experimental system, consisting of a feed tank, gear and vacuum pumps, VMD module, two heat exchangers for heating and cooling (i.e., heater and cooler, respectively), and distillate storage. Operational conditions are summarized in Table 2.

2.2.1. Experimental steps

The heater maintains the feed temperature at a constant value (between 26°C and 60°C) during VMD experiments. The temperature of the entering feed stream was recorded using a thermostat installed on each side the vessel. The gear pump supplies the hot feed solution to the VMD module, and the feed stream is distributed to lumen spaces of 180 hollow fiber membranes. The feed flow rate is set at 1.0 L/min, which provides a moderate lumen flow speed of 0.24 m/s. Using the lumen diameter of 0.7 mm, Reynolds number of this lumen flow is calculated as  $Re = 168$ , specifically at 25°C. The kinematic viscosity of water decreases

from 1.002 m<sup>2</sup>/s at 20°C to 0.475 m<sup>2</sup>/s at 60°C. But, due to the slow speed and small inner diameter of the hollow fiber, the thermal variation of the solution viscosity cannot change the lumen flow regime from laminar to turbulent. Feed solution passed through lumen spaces was returned and its temperature adjusted to the preset constant. This feed recirculation continued during VMD experiments until the proper amount of distillate was collected in the storage tank. The rare gas in the shell side of the module was continuously extracted using a vacuum pump, and therefore a low pressure (of 0.034 bar) was maintained in the shell side of the vessel. This gas flow contains water molecules, which were pre-evaporated at membrane-gas interfaces in lumen spaces. A condenser was installed between the membrane module and vacuum pump. The temperature of the cooling stream of the condenser is maintained at 4.5°C ± 0.5°C for fast condensation of the water vapor. This product water is collected in the distillate storage tank, located between the condenser and the vacuum pump. The salinity of the distillate water was measured using a refractometer (model: PAL-03S, Atago Co., Ltd., Japan). In all the experiments reported in this work, the produced distillate does not have any salinity.

3. Theoretical

3.1. Vapor pressure of saline waters

The vapor pressure of the saline water  $P_{v,sw}$  is often represented as a product of vapor pressure  $P_{v,w}(T)$  of pure water and a weighting function  $f(C)$  of saline concentration  $C$ :

$$P_{v,sw}(T, C) = P_{v,w}(T)f(C) \tag{1}$$

where  $f(C)$  should satisfy

$$f(C \rightarrow 0) = 1 \tag{2}$$

and  $T$  is temperature at the interface between liquid and gas phases, which is approximately equal to feed temperature when temperature polarization is moderate. Several empirical correlations were suggested for the weighting function  $f$  and an excellent review can be found elsewhere [7]. First, Emerson and Jamieson's correlation [25] was employed for  $f(C)$  such as

$$\log_{10}f(C) = -2.1609 \times 10^{-4}C - 3.5012 \times 10^{-7}C^2 \tag{3}$$

which is valid for 35 g/kg <  $C$  < 170.0 g/kg with error range of ±0.07%. An advantage of using Eq. (1) with (3) is that influences of temperature and concentration are separately contributed to the seawater saturation pressure as a product. Note that coefficients on the right side of Eq. (3) are all negative. The vapor pressure of saline water decreases with respect to the salt concentration. For  $C = 0, 34,$  and  $62$  g/kg,  $f(C)$  values are 1.0, 0.98231, and 0.96546, respectively. This indicates that the vapor pressures of DSW34 and DSW62 decreased 1.769% and 3.454% from that of fresh water, respectively. These variations with respect to the saline concentration do not depend on the solution temperature.

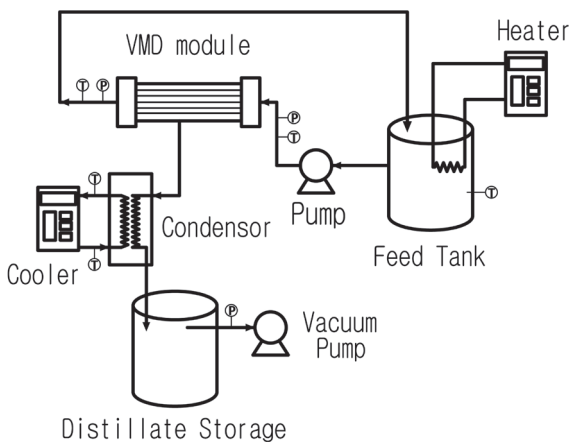


Fig. 2. Schematic of vacuum membrane distillation system.

Table 2  
Experimental conditions and parameters

	Variables	Values	Unit
Operation	Vacuum (shell) pressure, $P_{vac}$	0.031 – 0.037	bar
	Feed (lumen) temperature, $T_f$	26 – 61, $\Delta T = 5$	°C
	Initial feed volume	13	Liter
	Feed flow rate, $q_f$	1.0	liter/min
	Feed flow speed, $u_f$	0.24	m/sec
	Condenser temperature, $T_c$	4.5 ± 0.5	°C

Other expressions for the relative saturation pressure of seawater to that of fresh water include Raoult’s law (RL) [26], Millero (MR) [27], and Weiss and Price (WP) [28], as shown in Fig. 3. Specific formulas can be found elsewhere [7]. Raoult’s law has a form, similar to Eq. (1), that the saturation pressure ratio is independent of temperature. For 34 and 62 g/kg, the ratios are 0.9802 and 0.9635, respectively. Both Millero’s and Weiss and Price’s correlations are limited to temperatures between 0°C to 40°C and salinity between 0 to 40 g/kg. Therefore, these two correlations can be used only for seawater of salinity no more than 40 g/kg and temperatures below 40°C, above which abnormal behavior of Milleno’s correlation above 40°C is clearly shown in Fig. 3. Although it is stated that use of WP is likewise restricted, simple extrapolation of WP shows reasonable trends that the seawater saturation pressure decreases with salt concentration and it is either constant or decreasing with respect to temperature.

In the experiments, the vacuum pressure was maintained at  $0.034 \pm 0.003$  bar. Note that 26.25°C is the water temperature in equilibrium with the vapor pressure (0.034 bar). If the feed temperature of VMD is 26.25°C and the vacuum pressure is 0.034 bar, then the transmembrane gradient of the partial pressure is theoretically zero and no distillate flux will be generated. Zero or negligible distillate volume was observed under these conditions. (See the next section for details.) To evaporate saline water of finite concentration  $C (>0)$  and temperature  $T$ , a necessary (not sufficient) condition is that the vacuum pressure  $P_{vac}$  should be lower than the vapor pressure of pure water at a specific feed temperature, that is,  $P_{vac} < P_{v,sw}(T, C = 0)$ . Equivalently, the equilibrium temperature of the vacuum pressure (inversely calculated using a correlation equation of water vapor pressure with respect to temperature) should be lower than the feed temperature.

Accurate estimation with fundamental rigor of the water vapor pressure is an important issue in VMD modeling.

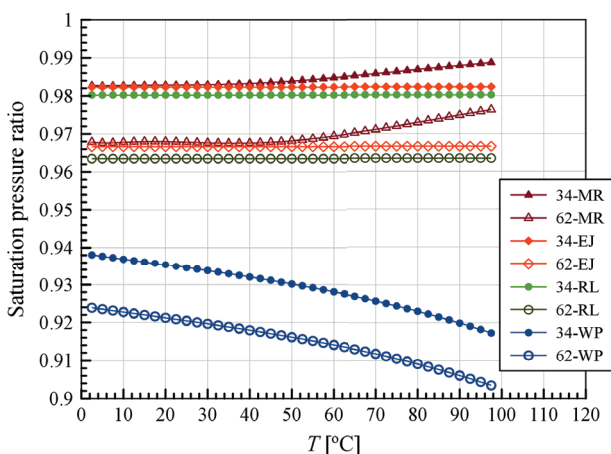


Fig. 3. Ratio of seawater saturation pressure with respect to temperature for concentrations of 34 g/kg and 62 g/kg, as indicated in the legend.

Note: MR, EJ, RL, and WP are correlations provided by Millero [27], Emerson and Jamieson [25], Raoult’s law [26], and Weiss and Price [28].

A newly developed representation of [29] was employed for the saturation pressure:

$$P_{v,w} = p_0 \exp\left[-\frac{L(T)}{RT}\right] \tag{4}$$

$$L(T) = l_0 + l_1 T \ln T \tag{5}$$

where  $p_0 = 2.71690 \times 10^{24}$  mmHg,  $l_0 = 57.075$  kJ/mol, and  $l_1 = 4.3856 \times 10^{-2}$  kJ/mol K. In Eq. (4), the coefficients of vapor pressure are fundamentally related to those of the latent heat of water:

$$l_w(T) = l_0 - l_1 T \tag{6}$$

In our previous work [29], Eq. (4) is directly derived using the Clausius–Clapeyron equation and the empirical correlation of the latent heat Eq. (6).

### 3.2. Distillate flux

The distillate flux can be written as follows:

$$J_w(T,C) = B\Delta P = B[P_{v,sw}(T, C) - P_{vac}] \tag{7}$$

where  $B$  is the mass transfer coefficient. Substitution of Eq. (1) into (7) provides the following:

$$J_w(T,C) = B(T)P_{v,w}(T,C)[f(C) - \hat{p}_{vac}] \tag{8}$$

$$\hat{p}_{vac} = -\frac{P_{vac}}{P_{v,w}(T)} \tag{9}$$

where  $P_{vac} = 0.034$  bar in the current study. Because  $B$  is related to only migration of vapor molecules through membrane pores, one can assume that  $B = B(T)$ , which is independent of  $C$ . The flux ratio of the DSW and DIW can be represented as follows:

$$j_{DSW} = \frac{J_w(T,C)}{J_w(T,0)} = \frac{f(C) - \hat{p}_{vac}}{1 - \hat{p}_{vac}} \tag{10}$$

which is in this study defined as the relative flux of DSW to DIW at temperature  $T$ . The dimensionless vacuum pressure  $\hat{p}_{vac}$  rapidly decreases with temperature because the water vapor pressure is highly non-linear with respect to  $T$  [29]. This means that the relative flux of DSW will reach the extreme value of  $f(C)$  as the temperature increases:

$$\lim_{high\ T} j_{DSW}(T) \rightarrow f(C) \tag{11}$$

Theoretically, at temperature  $T \rightarrow 100^\circ\text{C}$ , the vapor pressure reaches 1.01325 bar, and therefore  $\hat{p}_{max} \rightarrow 0.034/1.01325 = 0.03356$ ,

giving  $j_{DSW,max} = 0.9817$  and  $0.96426$  for DSW34 and DSW62, respectively. DSW fluxes cannot be higher than that of DIW, but their magnitudes are only a few percent less.

4. Results and discussion

Fig. 4(a) shows distillate fluxes of the three feed solutions (DIW, DSW34 and DSW62) with the feed temperature. As expected, fluxes are very low at 26°C, where the driving force is negligible. Only the DIW provides non-zero flux and no distillate volumes are collected for DSW34 and DSW62 solutions. At this temperature, the water vapor pressure is reported as 0.03364 bar [30], which is approximately equal to or slightly below the vacuum pressure of 0.034 bar. The onset temperature point of distillate fluxes seems to be around 31°C, above which fluxes monotonously increase with respect to temperature. Throughout the temperature range from 41°C to 60°C, DIW flux is higher than that of DSW34, followed by DSW62. Variations of distillate flux saline concentration are apparent, but their differences are small.

Fig. 4(b) shows the fluxes of DSW34 and DSW62 normalized by DIW flux. Due to the small driving force at low temperatures, flux ratios below 36°C appear to be influenced by experimental conditions or uncertainties and they do not seem to provide important physical meanings. Above 41°C, DSW34 has higher flux values than those of DSW62, as expected from Fig. 4(a). Observing the trend of Fig. 4(b), it is expected that the flux ratio rapidly increases from zero at 26°C and gradually reaches a plateau for higher temperatures. Emerson and Jamieson’s and Weiss and Price’s correlations were used to compare the simple theoretical prediction and experimental observations. The flux ratio of DSW34/DSW62 is plotted using solid/dashed lines, respectively. Asymptotic values are shown as the horizontal dash-dot and dash-double dot lines for DSW34 and DSW62, respectively. The EJ and WP theories predicted a much steeper increase in  $j_{DSW}$  with respect to the feed temperature than the experimental observations. Since  $j_{DSW}$  does not include any geometrical factors, it is valid for both flat sheet and hollow fiber modules. The quantitative disagreement between the theory and experiment must be from either inaccuracy of  $f(C)$  or  $\hat{p}_{vac}$ . It is interesting to see that what both EJ and WP predict about  $j_{DSW}$  does not show a noticeable difference in Fig. 4(b), whereas WP predicts a lower saturation pressure than EJ (as shown in Fig. 3). This implies that effects of salt concentration on seawater evaporation are minimal, and the flux decline is highly correlated to heat loss during VMD operation. However, the fundamental rigor and numerical accuracy of  $P_{v,w}(T)$  has been already confirmed. On the other hand, the temperature in Eq. (10) is interpreted as the temperature that water molecules evaporate at the lumen surfaces. This is because on lumen surfaces of the inside-out mode, the temperature can be maintained close to the feed temperature with some difference due to temperature polarization. The feed stream loses its thermal energy as it flows along the lumen interior. Although the vacuum has one order of magnitude smaller thermal conductivity than that of air, the heat loss through the cylindrical vessel cannot be fully negligible. Ambient heat influx to the vessel through the cylindrical vessel wall may change the effective evaporation temperature and hence DSW vapor pressure. Considering

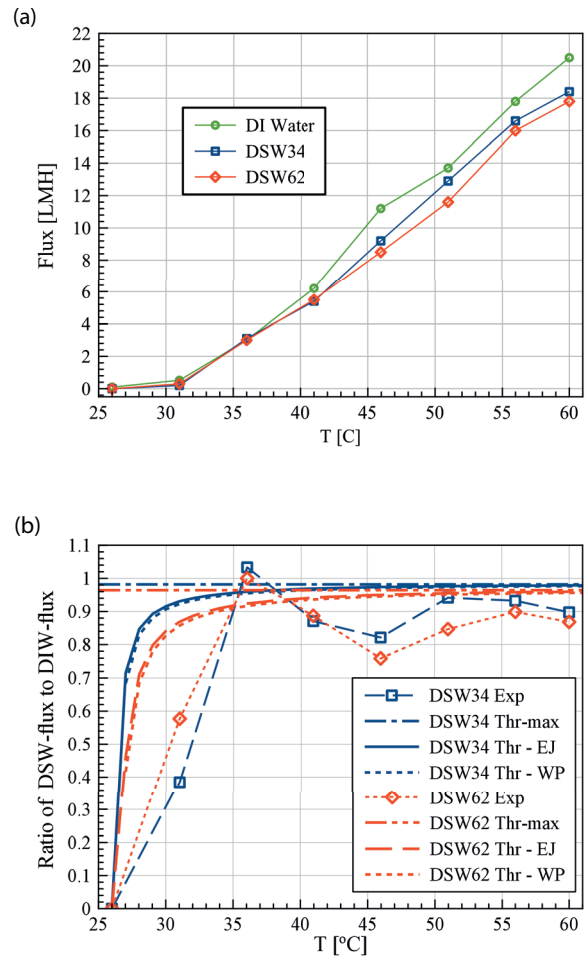


Fig. 4. (a) Total distillate flow rate per unit inner surface area and (b) ratios of DSW fluxes to DIW flux at various temperatures.

the above issues, we think that the solid and dashed lines in Fig. 4(b) must be translated to the right, being anchored at point (25°C, 0). If so, the theoretical lines drop down a little at each temperature, coming closer to the experimental data. In addition, the asymptotic values of  $j_{DSW}$  must decrease accordingly, as implied in Eq. (11). This theoretical analysis qualitatively predicted the convergence of two DSW fluxes at high temperatures, which is experimentally observed in Fig. 4(a) and implied in Fig. 4(b). This is because water molecules in the feed solution have more kinetic energy to break hydrogen bonds and evaporate more frequently to the gas phase. The hindering effect on water evaporation by salt ions in the feed solution becomes less significant at higher temperatures. This implies that the variation of vapor pressure by high salinity is insignificant at high feed temperatures, and the distillate flux is almost indifferent to the feed salinity. The performance of VMD is insignificantly influenced by the increases in seawater concentration as much as 200%. Thermal energy consumption to heat up the feed solution is almost independent of the feed concentration for the same distillate flux. This confirms the great potential of VMD on desalination and MCr. Technical aspects of MCr can be found elsewhere [18,19].

## 5. Concluding remarks

In this work, the practicality of MD in terms of concentrating DSW and its secondary RO brines were systematically investigated. The final goal of this research is to use VMD for crystallization of DSW minerals. Among several MD types, VMD is selected because of its superior performance and lower risk of the membrane wetting. During the series of VMD experiments, no-wetting was observed, and salt ions were completely (100%) rejected. Distillate flux decreased with respect to the feed concentration, but changes are small even when the high salinity solutions (34 g/kg and 62 g/kg) were used. A simple Eq. (10) is developed to predict or analyze distillate fluxes of high salinity solutions. This theory gives qualitatively good agreement with the experimental data. Heat flux across the vessel wall seems to play an important role in water evaporation on the lumen surfaces. The high salinity does not significantly change the vapor pressure of seawater and hence VMD distillate flux. Future use of VMD looks promising for concentrating high salinity water when combined with MCR.

## Acknowledgment

This work was financially supported by the National R&D project of “Development of new application technology for deep seawater industry”, funded by the Ministry of Oceans and Fisheries of the Republic of Korea.

## References

- [1] L. Camacho, L. Dumée, J. Zhang, J.-D. Li, M. Duke, J. Gomez, S. Gray, Advances in membrane distillation for water desalination and purification applications, *Water*, 5 (2013) 94–196.
- [2] T. Matsuura, M. Khayet, *Membrane distillation: principles and applications*, Elsevier: New York (2011).
- [3] R.B. Saffarini, E.K. Summers, H.A. Arafat, J.H. Lienhard V, Economic evaluation of stand-alone solar powered membrane distillation systems, *Desalination*, 299 (2012) 55–62.
- [4] A. Alkhudhiri, N. Darwish, N. Hilal, Membrane distillation: a comprehensive review, *Desalination*, 287 (2012) 2–18.
- [5] A.S. Kim, S.J. Ki, H.-J. Kim, Membrane distillation: multi-scale and multi-physics phenomena, *Desal. Wat. Treat.*, doi: 10.5004/dwt.2016.11423.
- [6] T.Y. Cath, D. Adams, A.E. Childress, Membrane contactor processes for wastewater reclamation in space, *J. Membr. Sci.*, 257 (2005) 111–119.
- [7] M.H. Sharqawy, J.H. Lienhard V, S.M. Zubair, Thermophysical properties of seawater: a review of existing correlations and data, *Desal. Wat. Treat.*, 16 (2010) 354–380.
- [8] A.C. Sun, W. Kosar, Y. Zhang, X. Feng, Vacuum membrane distillation for desalination of water using hollow fiber membranes, *J. Membr. Sci.*, 455 (2014) 131–142.
- [9] A. Criscuoli, M.C. Carnevale, E. Drioli, Evaluation of energy requirement in membrane distillation, *Chem. Eng. Process.* 47 (2008) 1098–1105.
- [10] A.S. Kim, H.-J. Kim, H.-S. Lee, S. Cha, Dual-use open cycle ocean thermal energy conversion (OC-OTEC) using multiple condensers for adjustable power generation and seawater desalination, *Renew. Energy*, 85 (2016) 344–358.
- [11] A.S. Kim, W. Oh, H.-S. Lee, S. Cha, H.J. Kim, Perspective of membrane distillation applied to ocean thermal energy conversion, *IDA J. Desal. Water Reuse*, 7 (2015) 17–24.
- [12] N. Ghaffour, T.M. Missimer, G.L. Amy, Technical review and evaluation of the economics of water desalination: current and future challenges for better water supply sustainability, *Desalination*, 309 (2013) 197–207.
- [13] X. Ji, E. Curcio, E. Drioli, S. Al Obaidani, G. Di Profio, E. Fontananova, Membrane distillation-crystallization of seawater reverse osmosis brines, *Sep. Purif. Technol.*, 71 (2010) 76–82.
- [14] M. Schorr, B. Valdez, J. Ocampo, A. Eliezer, Corrosion Control in the Desalination Industry, *Desalination, Trends and Technologies*, INTECH, New York, NY, 2011.
- [15] Y. Wu, E. Drioli, The behaviour of membrane distillation of concentrated aqueous solution, *Water Treat.*, 4 (1989) 399–415.
- [16] E. Curcio, A. Criscuoli, E. Drioli, Membrane crystallizers, *Ind. Eng. Chem. Res.* 40 (2001) 2679–2684.
- [17] E. Drioli, E. Curcio, A. Criscuoli, G. di Profio, Integrated system for recovery of  $\text{CaCO}_3$ ,  $\text{NaCl}$  and  $\text{MgSO}_4 \cdot 7\text{H}_2\text{O}$  from nanofiltration retentate, *J. Membr. Sci.*, 239, (2004) 27–38.
- [18] E. Curcio, E. Drioli, G. Di Profio, Progress in membrane crystallization, *Curr. Opinion Chem. Eng.*, 1 (2012) 178–182.
- [19] E. Drioli, E. Curcio, G. di Profio, State of the art and recent progresses in membrane contactors, *Chem. Eng. Res. Design*, 83 (2005) 223–233.
- [20] D.S. Moon, D.H. Jung, H.J. Kim, P.K. Shin, Comparative analysis on resources characteristics of deep ocean water and brine groundwater, *Korea Soc. Marine Environ. Energy*, 2 (2004) 42–46.
- [21] C.-L. Hsu, Y.-Y. Chang, C.-H. Chiu, K.-T. Yang, Y. Wang, S.-G. Fu, Y.-C. Chen, Cardiovascular protection of deep-seawater drinking water in high-fat/cholesterol fed hamsters, *Food Chem.*, 127 (2011) 1146–1152.
- [22] K.Y. Choi, Y.I. Kim, Stability evaluation of deep sea water intake areas in Gangwon region, East Sea, *J. Korean Soc. Marine Environ. Energy*, 5 (2015) 205–208.
- [23] L. Eykens, I. Hitsov, K. De Sitter, C. Dotremont, L. Pinoy, I. Nopens B. Van der Bruggen, Influence of membrane thickness and process conditions on direct contact membrane distillation at different salinities, *J. Membr. Sci.*, 498 (2016) 353–364.
- [24] A.S. Kim, Cylindrical cell model for direct contact membrane distillation (DCMD) of densely packed hollow fibers, *J. Membr. Sci.*, 455 (2014) 168–186.
- [25] W.H. Emerson, D.T. Jamieson, Some physical properties of sea water in various concentrations, *Desalination*, 3 (1967) 213–224.
- [26] L. d. Landau, E.M. Lifshitz, *Statistical physics*, 3rd ed., Part 1, *Course of theoretical physics*, Vol. 5, Pergamon Press: New York (1980).
- [27] F.J. Millero, *The sea*, Vol. 5, John Wiley: New York (1974), pp. 3–80.
- [28] R.F. Weiss, B.A. Price, Nitrous oxide solubility in water and seawater, *Marine Chem.*, 8 (1980) 347–359.
- [29] A.S. Kim, A two-interface transport model with pore-size distribution for predicting the performance of direct contact membrane distillation (DCMD), *J. Membr. Sci.*, 428 (2013) 410–424.
- [30] W.M. Haynes (Ed.), *CRC handbook of chemistry and physics*, 96th ed., Taylor & Francis Group: Boca Raton, FL (2015).